https://doi.org/10.1016/j.jorganchem.2019.04.026



# Synthesis, characterization and photovoltaic properties of platinum-containing poly(aryleneethynylene) polymers with electron-deficient diketopyrrolopyrrole unit

**Hongmei Zhan [a,b,*], Qian Liu [a,c,*], Shu-Kong So [d], Wai-Yeung Wong [a,e,*]**

[a] *Department of Chemistry, Hong Kong Baptist University, Waterloo Road, Kowloon Tong, Hong Kong, P.R. China.*

[b] *State Key Laboratory of Polymer Physics and Chemistry, Changchun Institute of Applied Chemistry, Chinese Academy of Sciences, Changchun, 130022, P.R. China. E-mail: hmzhan@ciac.ac.cn*

[c] *College of Biological and Chemical Engineering, Anhui Polytechnic University, Wuhu, Anhui 241000, P.R. China. E-mail: lqcz_2008@163.com*

[d] *Department of Physics, Hong Kong Baptist University, Waterloo Road, Kowloon Tong, Hong Kong, P.R. China*

[c] *Department of Applied Biology and Chemical Technology, The Hong Kong Polytechnic University, Hung Hom, Hong Kong, P.R. China. E-mail: wai-yeung.wong@polyu.edu.hk*

**Abstract**

Three new solution-processable Pt(II)-containing poly(aryleneethynylene) polymers based on diketopyrrolopyrrole moiety and their corresponding diplatinum model complexes were synthesized via the Sonogashira-type coupling reaction of the platinum(II) chloride precursor and each of the diethynyl ligands. The photophysical, thermal stability, electrochemical, carrier mobility and photovoltaic properties of these polymers were fully investigated. These polymers exhibit strong absorption bands in the range of 550−750 nm, and fluorescent bands between 650 and 850 nm. One thiophene flanked diketopyrrolopyrrole based polymer with linear *n*-octyl chains shows a better photovoltaic performance than that made from the branched 2-ethylhexyl analogue.

**Keywords:** Diketopyrrolopyrrole / metallopolymer / platinum / photovoltaics / solar cell

## 1. Introduction

Bulk heterojunction (BHJ) organic solar cells containing conjugated polymer donor and fullerene/non-fullerene acceptor materials have attracted most of attention due to their potential applications in flexible, light-weight and large-scale devices at low-cost [1−6]. Through the continuous efforts on the materials design [7−10], morphology control [11−14] and device engineering such as inverted and/or tandem solar cells [15−19], the power conversion efficiency (PCE) has reached over 14% in recent years [20−22]. The development of novel electron-donating polymeric materials plays a key role in these great advances. The efficient design concepts mainly include alternating subunits with electron-rich and electron-deficient properties along the polymer main chain and enhancing the stability of quinoidal structure and coplanarity of the main chain. In addition, another representative and versatile approach in designing polymers is introducing the metal center into the conjugated polymeric backbone, based on the efficient intersystem crossing (ISC) between the singlet and triplet energy levels of heavy metal and the longer lifetime of triplet excitons, which may be beneficial for increasing the excited state lifetime of conjugated main chain and thus improving the photovoltaic efficiency. Although several Pt-containing poly(aryleneethynylene)s have shown good photovoltaic performance [23−25], there are still many unexplored aspects in the organometallic polymer-based BHJ solar cells. Therefore, it is necessary to thoroughly understand the working principle of this type of solar cells and further refine the device efficiency.

Conjugated polymers with donor-acceptor (D-A) architectures and narrow

bandgaps possess broad absorption spectrum and strong intramolecular charge transfer (ICT) interaction between the donor (D) and acceptor (A) units. The optical and electronic properties of conjugated D-A polymers could be readily tuned through careful design and selection of D and A building blocks. Diketopyrrolopyrrole (DPP) has a planar conjugated bicyclic structure, which leads to strong π-π interactions, and the lactam part makes the DPP unit to exhibit a strong electron-withdrawing effect. Therefore, the DPP unit can be used as a potential electron-accepting unit in the design of optoelectronic materials. The solubility of DPP-based polymer can be significantly tuned by modifying the 2,5-positions of the DPP moiety (N atoms in the lactam) with solubilizing alkyl chains (either straight or branched chain). Such properties of easy modification can also be beneficial to get solution processable materials.

DPP-based conjugated materials have raised considerable attention for their extensive applications in solar cells as well as in organic field-effect transistors (OFET) [26−30], exhibiting excellent ambipolar charge transport properties with high hole and electron mobilities in the latter. A number of DPP-based copolymers with alternating electron-deficient DPP units and different electron-rich units such as thiophene, furan, fluorene, carbazole, cyclopentadithiophene, dithienosilole, benzo[1,2-*b*:3,4-*b*]dithiophene, benzo[1,2-*b*:3,4-*b'*]dithiophene, and dithieno[3,2-*b*:2',3'-*d*]pyrrole commonly used in the field of organic solar cells have been reported [31−34]. These polymers exhibit better photovoltaic performance and high hole mobility [35,36]. Moreover, some small molecules containing DPP moieties

were also used as p-type materials in solution-processed small-molecule solar cells with PCE of 8% [37,38].

Given all the considerations above, we report here the synthesis and characterization of a series of new conjugated organometallic D-A polymers with alternating thiophene-flanked DPP moieties and *trans*-$Pt(PBu_3)_2$ acetylide units (**P1**−**P3** in Fig. 1). The solubility of DPP polymers was tuned by introducing different alkyl groups (straight *n*-octyl or branched 2-ethylhexyl (EH)) and the π-electron conjugation length of polymer main chain could be extended by adding the 3-hexylthiophene ring with the aim of improving their visible absorption properties. Studies of the photophysical, thermal stability and electrochemical properties of these platinum(II)-containing polyyne polymers were conducted, and their photovoltaic properties were investigated by fabricating solution-processed BHJ devices consisting of these polymers and [6,6]-phenyl-$C_{61}$-butyric acid methyl ester (PCBM). Polymer **P1** with linear side chain exhibits better photovoltaic performance compared to the branched counterparts.

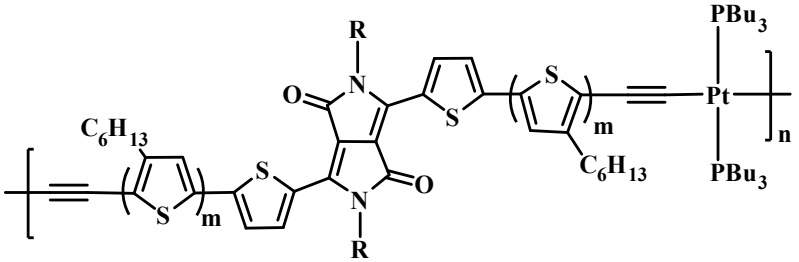


R = *n*-$C_8H_{17}$, m = 0 **P1**
R = 2-ethylhexyl, m = 0 **P2**
R = 2-ethylhexyl, m = 1 **P3**

**Fig. 1.** Chemical structures of DPP-based Pt(II) polyyne polymers **P1**−**P3**.

## 2. Materials and methods

### *2.1. Materials and instruments*

All reactions were carried out under a nitrogen atmosphere by using standard Schlenk techniques. Solvents were dried and distilled from appropriate drying agents under an inert atmosphere prior to use. All reagents and chemicals, unless otherwise stated, were purchased from commercial sources and used without further purification. *trans*-$Pt(PEt_3)_2(Ph)Cl$ [39] and *trans*-$Pt(PBu_3)_2Cl_2$ [24] were prepared according to the literature methods. All reactions were monitored by thin-layer chromatography (TLC) with Merck pre-coated glass plates. Flash column chromatography and preparative TLC were carried out using silica gel from Merck (230–400 mesh).

Infrared spectra were recorded as dichloromethane ($CH_2Cl_2$) solutions using a Perkin-Elmer Paragon 1000 PC or Nicolet Magna 550 Series II FT-IR spectrometer, using $CaF_2$ cells with a 0.5 mm path length. Fast atom bombardment (FAB) mass spectra were recorded on a Finnigan MAT SSQ710 system and MALDI-TOF (matrix-assisted laser desorption/ionization time-of-flight) spectra were obtained by a Autoflex Bruker MALDI-TOF mass spectrometer. NMR spectra were measured in $CDCl_3$ on a Varian Inova 400 MHz FT-NMR spectrometer and chemical shifts are quoted relative to tetramethylsilane for $^{1}H$ and $^{13}C$ nuclei and $H_3PO_4$ for $^{31}P$ nucleus.

The cyclic voltammograms were acquired with a CHI model 600D electrochemistry station in deoxygenated acetonitrile containing 0.1 M $[Bu_4N]PF_6$ as the supporting electrolyte. A conventional three-electrode configuration consisting of

a platinum working electrode, a Pt-wire counter electrode and a Ag/AgCl reference electrode was used. The polymer films were casted on the ITO covered glass. The highest occupied molecular orbital (HOMO) and the lowest unoccupied molecular orbital (LUMO) levels of the polymers were calculated according to the following equations $E_{HOMO} = -(E_{ox} + 4.72)$ eV and $E_{LUMO} = -(E_{red} + 4.72)$ eV, respectively. All potentials reported were quoted with reference to the ferrocene-ferrocenium ($Fc/Fc^+$) couple at a scan rate of 100 mV $s^{-1}$.

*2.2. Synthesis*

*2.2.1. Synthesis of **L1-T** and **L2-T***

**L1-T**: A mixture of 3,6-bis-(thienyl)-diketopyrrolopyrrole (**DPPT**) (362 mg, 1.21 mmol), potassium carbonate ($K_2CO_3$, 556 mg, 4.03 mmol) and 1-bromooctane (778 mg, 4.03 mmol) in 12 mL of dried dimethylformamide (DMF) was heated at 120 °C overnight. After being cooled to room temperature, the resulting mixture was poured into water (50 mL) and extracted with $CH_2Cl_2$. The combining organic layer was dried with anhydrous sodium sulfate, and concentrated under reduced pressure. The residue was recrystallized from the solvent mixture of $CH_2Cl_2$ and methanol to give the product **L1-T** as a deep red solid (319 mg, 50%). $^1$H NMR (400 MHz, $CDCl_3$, δ/ppm): 8.92 (dd, $J_1$ = 1.0 Hz, $J_2$ = 3.9 Hz, 2H, Ar), 7.64 (dd, $J_1$ = 1.0 Hz, $J_2$ = 5.0 Hz, 2H, Ar), 7.28 (dd, $J_1$ = 4.0 Hz, $J_2$ = 5.0 Hz, 2H, Ar), 4.07 (t, $J$ = 8.0 Hz, 4H, $C_8H_{17}$), 1.78−1.70 (m, 4H, $C_8H_{17}$), 1.45−1.38 (m, 4H, $C_8H_{17}$), 1.35−1.26 (m, 16H, $C_8H_{17}$), 0.87 (t, $J$ = 7.0 Hz, 6H, $C_8H_{17}$); $^{13}$C NMR (100 MHz, $CDCl_3$, δ/ppm): 161.39 (C=O), 140.03, 135.25, 130.66, 129.80, 128.61, 107.71 (Ar), 42.24, 31.77, 29.96, 29.21,

29.19, 26.88, 22.63, 14.09 ($C_8H_{17}$); FAB-MS: *m/z* 524.1 $[M]^+$.

The similar procedure was used to prepare **L2-T**.

**L2-T**: Deep red solid, yield: 46%. $^1$H NMR (400 MHz, $CDCl_3$, δ/ppm): 8.89 (dd, $J_1$ = 0.8 Hz, $J_2$ = 3.8 Hz, 2H, Ar), 7.63 (dd, $J_1$ = 0.8 Hz, $J_2$ = 3.8 Hz, 2H, Ar), 7.27 (dd, $J_1$ = 4.1 Hz, $J_2$ = 4.8 Hz, 2H, Ar), 4.08−3.97 (m, 4H, EH), 1.86−1.85 (m, 2H, EH), 1.41−1.22 (m, 16H, EH), 0.89−0.88 (m, 12H, EH); $^{13}$C NMR (100 MHz, $CDCl_3$, δ/ppm): 161.76 (C=O), 140.43, 135.28, 130.53, 129.83, 128.43, 107.92 (Ar), 45.85, 39.07, 30.21, 28.35, 23.53, 23.06, 14.03, 10.48 (EH). FAB-MS: *m/z* 524.3 $[M]^+$.

*2.2.2. Synthesis of **L1-Br** and **L2-Br***

**L1-Br**: **L1-T** (140 mg, 0.27 mmol) and 20 mL chloroform were added to a 50 mL round bottom flask equipped with a stirring bar and a condenser. Bromine (90 mg, 0.56 mmol) was added dropwise to the flask at room temperature. After stirring at room temperature for 10 min, the reaction mixture was heated to 60 °C and stirred for an additional hour. After cooling, the reaction mixture was poured into water (45 mL) and extracted with $CH_2Cl_2$. The combined organic layer was dried over anhydrous sodium sulfate, filtered and concentrated under reduced pressure. The crude product was recrystallized from the solvent mixture of $CH_2Cl_2$ and methanol to give the product **L1-Br** as a purple solid (156 mg, 86%). $^1$H NMR (400 MHz, $CDCl_3$, δ/ppm): 8.68 (d, *J* = 4.2 Hz, 2H, Ar), 7.24 (d, *J* = 4.2 Hz, 2H, Ar), 3.98 (t, *J* = 7.9 Hz, 4H, $C_8H_{17}$), 1.73−1.68 (m, 4H, $C_8H_{17}$), 1.41−1.25 (m, 20H, $C_8H_{17}$), 0.88 (t, *J* = 7.0 Hz, 6H, $C_8H_{17}$); $^{13}$C NMR (100 MHz, $CDCl_3$, δ/ppm): 161.05 (C=O), 139.01, 135.36, 131.66,

131.11, 119.16, 107.82 (Ar), 53.43, 42.29, 31.76, 29.98, 29.15, 26.82, 22.63, 14.10 ($C_8H_{17}$); FAB-MS: *m/z* 681.9 $[M]^+$.

The similar procedure was used to prepare **L2-Br**.

**L2-Br**: Purple solid, yield: 81%. $^1$H NMR (400 MHz, $CDCl_3$, δ/ppm): 8.66 (d, *J* = 4.2 Hz, 2H, Ar), 7.22 (d, *J* = 4.2 Hz, 2H, Ar), 3.99−3.88 (m, 4H, EH), 1.83−1.82 (m, 2H, EH), 1.39−1.24 (m, 16H, EH), 0.90−0.85 (m, 12H, EH); $^{13}$C NMR (100 MHz, $CDCl_3$, δ/ppm): 161.38 (C=O), 139.38, 135.42, 131.46, 131.11, 119.04, 107.94 (Ar), 45.96, 39.05, 30.10, 28.26, 23.48, 23.03, 14.04, 10.43 (EH). FAB-MS: *m/z* 682.2 $[M]^+$.

*2.2.3. Synthesis of **L3-HT***

$Pd(PPh_3)_4$ (13 mg, 0.011 mmol) was added into a solution of compound **L2-Br** (150 mg, 0.22 mmol) and tributyl(4-hexylthiophen-2-yl)stannane (312 mg, 0.68 mmol) in dry toluene (20 mL) under the nitrogen atmosphere. The reaction mixture was refluxed for 1−2 days. Once the reaction was completed based on TLC monitoring, the solvent was removed. The residue was purified by silica gel column chromatography eluting with $CH_2Cl_2$/hexane (1:1.5) to give the compound **L3-HT** (164 mg, 87%) as a purple solid. $^1$H NMR (400 MHz, $CDCl_3$, δ/ppm): 8.90 (d, *J* = 4.1 Hz, 2H, Ar), 7.28 (d, *J* = 4.1 Hz, 2H, Ar), 7.15 (s, 2H, Ar), 6.92 (s, 2H, Ar), 4.10−3.99 (m, 4H, EH), 2.61 (t, *J* = 7.6 Hz, 4H, $C_6H_{13}$), 1.92−1.91 (m, 2H, EH), 1.68−1.60 (m, 4H, $C_6H_{13}$), 1.53−1.28 (m, 28H, $C_6H_{13}$+EH), 0.93−0.86 (m, 18H, $C_6H_{13}$+EH); $^{13}$C NMR (100 MHz, $CDCl_3$, δ/ppm): 161.63 (C=O), 144.67, 143.14, 139.44, 136.63, 135.81, 127.87, 126.45, 124.44, 121.06, 108.21 (Ar), 45.93, 39.94, 31.66, 30.46, 30.38, 28.98, 28.60, 23.67,

23.15, 22.62, 14.12, 10.58 ($C_6H_{13}$+EH). FAB-MS: *m/z* 856.5 $[M]^+$.

*2.2.4. Synthesis of **L3-Br***

*N*-Bromosuccinimide (NBS) (36 mg, 0.20 mmol) was added to a solution of compound **L3-HT** (86 mg, 0.1 mmol) in chloroform (15 mL), and the reaction mixture was stirred overnight at room temperature in the dark. Once the reaction was completed based on TLC monitoring, the solvent was removed. The residue was purified by column chromatography on silica gel eluting with $CH_2Cl_2$/hexane (1:2) and precipitated from the solvent mixture of $CH_2Cl_2$ and methanol to give the pure product **L3-Br** (85 mg, 85%) as a deep purple solid. $^1$H NMR (400 MHz, C $CDCl_3$, δ/ppm): 8.87−8.84 (m, 2H, Ar), 7.20−7.19 (m, 2H, Ar), 7.00−6.98 (m, 2H, Ar), 4.07−4.98 (m, 4H, EH), 2.57−2.54 (m, 4H, $C_6H_{13}$), 1.90−1.88 (m, 2H, EH), 1.64−1.57 (m, 4H, $C_6H_{13}$), 1.39−1.28 (m, 28H, $C_6H_{13}$+EH), 0.92−0.86 (m, 18H, $C_6H_{13}$+EH); $^{13}$C NMR (100 MHz, $CDCl_3$, δ/ppm): 161.56 (C=O), 143.56, 141.91, 139.32, 136.50, 135.56, 128.18, 125.77, 124.56, 110.01, 108.40 (Ar), 45.93, 39.22, 31.59, 30.34, 29.63, 29.58, 28.91, 28.57, 23.65, 23.12, 22.59, 14.11, 10.55 ($C_6H_{13}$+EH); FAB-MS: *m/z* 1014.3 $[M]^+$.

*2.2.5. Synthesis of **L1-TMS**, **L2-TMS** and **L3-TMS***

**L1-TMS**: To an ice-cooled mixture of **L1-Br** (199 mg, 0.29 mmol) in freshly distilled triethylamine (10 mL) and $CH_2Cl_2$ (30 mL) solution mixture was added CuI (5 mg, 0.015 mmol), $Pd(OAc)_2$ (5 mg, 0.015mmol) and $PPh_3$ (20 mg, 0.044 mmol). After the

solution was stirred for 30 min at 0 °C, trimethylsilylacetylene (0.15 mL, 0.87 mmol) was added and the suspension was stirred for 30 min in an ice-bath before being warmed to room temperature. After reacting for 30 min at room temperature, the mixture was heated to 64 °C for 1−2 days. Once the reaction was completed based on TLC monitoring, the solvent mixture was evaporated under reduced pressure. The crude product was purified by column chromatography on silica gel with a solvent combination of $CH_2Cl_2$/hexane (1:1.5) as eluent to provide the pure product **L1-TMS** (148 mg, 71%) as a purple solid. $^1$H NMR (400 MHz, $CDCl_3$, δ/ppm): 8.86 (d, *J* = 4.1 Hz, 2H, Ar), 7.33 (d, *J* = 4.1 Hz, 2H, Ar), 4.03 (t, *J* = 7.9 Hz, 4H, $C_8H_{17}$), 1.74−1.60 (m, 4H, $C_8H_{17}$), 1.43−1.27 (m, 20H, $C_8H_{17}$), 0.88 (t, *J* =7.0 Hz, 6H, $C_8H_{17}$), 0.29 (s, 18H, TMS); $^{13}$C NMR (100 MHz, $CDCl_3$, δ/ppm): 161.40 (C=O), 139.45, 135.58, 134.04, 130.61, 128.71, 108.96, 104.62 (Ar), 96.91, 77.62 (C≡C), 42.61, 32.05, 30.28, 29.45, 29.43, 27.12, 22.91, 14.40 ($C_8H_{17}$), 0.28 (TMS); FAB-MS: *m/z* 716.2 $[M]^+$.

The same procedures were applied to prepare compounds **L2-TMS** and **L3-TMS**.

**L2-TMS:** Purple solid, yield: 83%. $^1$H NMR (400 MHz, $CDCl_3$, δ/ppm): 8.82 (d, *J* = 4.2 Hz, 2H, Ar), 7.32 (d, *J* = 4.2 Hz, 2H, Ar), 4.01−3.94 (m, 4H, EH), 1.86−1.84 (m, 2H, EH), 1.39−1.22 (m, 16H, EH), 0.90−0.85 (m, 12H, EH), 0.29 (s, 18H, TMS); $^{13}$C NMR (100 MHz, $CDCl_3$, δ/ppm): 161.77 (C=O), 139.87, 135.56, 133.84, 130.71, 128.62, 109.14 (Ar), 104.52, 96.94 (C≡C), 46.34, 39.33, 30.39, 28.61, 23.80, 23.34, 14.33, 10.71 (EH), −0.0035 (TMS). FAB-MS: *m/z* 716.4 $[M]^+$.

**L3-TMS:** Deep purple solid, yield: 77%. $^1$H NMR (400 MHz, $CDCl_3$, δ/ppm): 8.89 (d,

*J* = 4.2 Hz, 2H, Ar), 7.28 (d, *J* = 4.2 Hz, 2H, Ar), 7.05 (s, 2H, Ar), 4.05−4.02 (m, 4H, EH), 2.67 (d, *J* = 7.4 Hz, 4H, $C_6H_{13}$), 1.90 (m, 2H, EH), 1.66−1.61 (m, 4H, $C_6H_{13}$), 1.53−1.29 (m, 28H, $C_6H_{13}$+EH), 0.92−0.86 (m, 18H, $C_6H_{13}$+EH), 0.26 (s, 18H, TMS); $^{13}$C NMR (100 MHz, $CDCl_3$, δ/ppm): 161.69 (C=O), 150.12, 142.27, 139.40, 136.69, 135.76, 128.50, 125.98, 125.08, 119.16, 108.62 (Ar), 103.64, 96.98 (C≡C), 46.05, 39.32, 31.64, 30.43, 30.07, 29.66, 28.98, 28.65, 23.75, 23.22, 22.69, 14.21, 10.66 ($C_6H_{13}$+EH), 0.10 (TMS). FAB-MS: *m/z* 1049.5 $[M+H]^+$.

*2.2.6. Synthesis of ligands **L1**, **L2** and **L3***

**L1:** To a solution of **L1-TMS** (80 mg, 0.11 mmol) in 8 mL of $CH_2Cl_2$ and 5 mL of methanol was added $K_2CO_3$ (33 mg, 0.24 mmol) and the mixture was stirred for 4−5 h at room temperature under the nitrogen atmosphere. Once the reaction was completed based on TLC monitoring, the mixture was poured into 20 mL water and the organic phase was extracted by $CH_2Cl_2$. The combined organic layer was washed with saturated brine, dried over anhydrous sodium sulfate, filtered and concentrated under reduced pressure. The crude product was recrystallized from $CH_2Cl_2$ and methanol to give a purple solid of **L1** (47 mg, 75%). $^1$H NMR (400 MHz, $CDCl_3$, δ/ppm): 8.88 (d, *J* = 4.1 Hz, 2H, Ar), 7.40 (d, *J* = 4.1 Hz, 2H, Ar), 4.03 (t, *J* = 7.9 Hz, 4H, $C_8H_{17}$), 3.60 (s, 2H, C≡CH), 1.74−1.71 (m, 4H, $C_8H_{17}$), 1.42−1.28 (m, 20H, $C_8H_{17}$), 0.87 (t, *J* = 7.0 Hz, 6H, $C_8H_{17}$); $^{13}$C NMR (100 MHz, $CDCl_3$, δ/ppm): 161.12 (C=O), 139.26, 135.20, 134.20, 130.64, 127.16, 108.78 (Ar), 85.58, 76.23 (C≡C), 42.35, 31.76, 30.01, 29.16, 26.83, 22.63, 14.10 ($C_8H_{17}$); FAB-MS: *m/z* 572.4 $[M]^+$; IR (KBr):

$\nu$(C≡C) 2094 $cm^{-1}$.

The same procedures were applied to prepare other ligands **L2** and **L3**.

**L2**: Purple solid, yield: 82%. $^{1}$H NMR (400 MHz, $CDCl_3$, δ/ppm): 8.84 (d, $J$ = 4.1 Hz, 2H, Ar), 7.38 (d, $J$ = 4.1 Hz, 2H, Ar), 4.00−3.97 (m, 4H, EH), 3.60 (s, 2H, C≡CH), 1.85−1.84 (m, 2H, EH), 1.37−1.25 (m, 16H, EH), 0.90−0.87 (m, 12H, EH); $^{13}$C NMR (100 MHz, $CDCl_3$, δ/ppm): 161.45 (C=O), 139.64, 135.24, 134.05, 130.71, 127.04, 108.91 (Ar), 85.51, 76.26 (C≡C), 46.02, 39.11, 30.09, 28.25, 23.47, 23.05, 14.03, 10.43 (EH); FAB-MS: *m/z* 573.5 $[M+H]^+$; IR (KBr): $\nu$(C≡C) 2098 $cm^{-1}$.

**L3**: Deep purple solid, yield: 77%. $^{1}$H NMR (400 MHz, $CDCl_3$, δ/ppm): 8.88 (d, $J$ = 4.2 Hz, 2H, Ar), 7.29 (d, $J$ = 4.2 Hz, 2H, Ar), 7.06 (s, 2H, Ar), 4.09−3.98 (m, 4H, EH), 3.57 (s, 2H, C≡CH), 2.69 (d, $J$ = 7.6 Hz, 4H, $C_6H_{13}$), 1.90−1.89 (m, 2H, EH), 1.66−1.61 (m, 4H, $C_6H_{13}$), 1.37−1.25 (m, 28H, $C_6H_{13}$+EH), 0.93−0.89 (m, 18H, $C_6H_{13}$+EH). $^{13}$C NMR (100 MHz, $CDCl_3$, δ/ppm): 161.61 (C=O), 150.36, 141.96, 139.35, 136.55, 136.06, 128.54, 125.80, 125.12, 117.74, 108.57(Ar), 85.35, 76.26 (C≡C), 45.96, 39.24, 31.58, 30.34, 30.08, 29.55, 28.93, 28.56, 23.66, 23.12, 22.59, 14.10, 10.56 (EH+$C_6H_{13}$); FAB-MS: *m/z* 905.4 $[M+H]^+$; IR (KBr): $\nu$(C≡C) 2091 $cm^{-1}$.

*2.2.7. Synthesis of polymers **P1**, **P2** and **P3***

A typical procedure for the synthesis of **P1** starting from **L1** is illustrated as follows: The solution mixture of **L1** (32 mg, 0.05 mmol), *trans*-$Pt(PBu_3)_2Cl_2$ (37 mg, 0.05 mmol) and CuI (3.00 mg) in triethylamine (5 mL) and dry $CH_2Cl_2$ (10 mL) was

stirred at room temperature under the nitrogen atmosphere for 24 hours. The solvents were evaporated under reduced pressure. The residue was dissolved in $CH_2Cl_2$ and filtered through a short neutral aluminum column using the same eluent to remove ionic impurities and catalyst residues. After removal of the solvent, the crude product was purified by precipitation in methanol from $CH_2Cl_2$. The precipitate was collected via filtration and washed with a copious amount of methanol and dried under vacuum for 5 h to give the pure product **P1** (45 mg, 74%) as a deep purple solid. $^1$H NMR (400 MHz, $CDCl_3$, δ/ppm): 8.99−8.98 (m, 2H, Ar), 7.00−6.96 (m, 2H, Ar), 4.05−4.03 (m, 4H, $C_8H_{17}$), 2.14−2.00 (m, 12H, $PBu_3$), 1.73−1.68 (m, 4H, $C_8H_{17}$),1.63−1.57 (m, 12H, $PBu_3$),1.50−1.38 (m, 12H, $PBu_3$), 1.31−1.25 (m, 20H, $C_8H_{17}$), 0.99−0.94 (m, 18H, $PBu_3$), 0.88 (t, $J$ =7.0 Hz, 6H, $C_8H_{17}$); $^{31}$P NMR (162 MHz, $CDCl_3$, δ/ppm): 3.76 ($^1J_{P–Pt}$ = 2306 Hz); IR (KBr): $\nu$(C≡C) 2079 cm$^{-1}$.

**P2**: Deep purple solid, yield: 75%. $^1$H NMR (400 MHz, $CDCl_3$, δ/ppm): 8.98 (d, $J$ = 3.6 Hz, 2H, Ar), 6.96 (d, $J$ = 3.6 Hz, 2H, Ar), 4.00−3.99 (m, 4H, EH), 2.18−2.10 (m, 12H, $PBu_3$), 1.97−1.92 (m, 2H, EH), 1.61−1.56 (m, 12H, $PBu_3$), 1.52−1.43 (m, 12H, $PBu_3$), 1.37−1.25 (m, 16H, EH), 0.96−0.87 (m, 30H, $PBu_3$+EH); $^{31}$P NMR (162 MHz, $CDCl_3$, δ/ppm): 3.74 ($^1J_{P–Pt}$ = 2302 Hz); IR (KBr): $\nu$(C≡C) 2079 cm$^{-1}$.

**P3**: Deep green solid, yield: 68%. $^1$H NMR (400 MHz, $CDCl_3$, δ/ppm): 8.93 (d, $J$ = 3.7 Hz, 2H, Ar), 7.19 (d, $J$ = 3.5 Hz, 2H, Ar), 7.04 (s, 2H, Ar), 4.10−3.97 (m, 4H, EH), 2.68−2.59 (m, 4H, $C_6H_{13}$), 2.20−2.09 (m, 12H, $PBu_3$), 2.02−1.90 (m, 2H, EH), 1.73−1.40 (m, 28H, $PBu_3$+$C_6H_{13}$), 1.39−1.25 (m, 28H, $C_6H_{13}$+EH), 0.97−0.88 (m, 36H, $PBu_3$+$C_6H_{13}$+EH); $^{31}$P NMR (162 MHz, $CDCl_3$, δ/ppm): 3.58 ($^1J_{P–Pt}$ = 2332 Hz)

ppm; IR (KBr): $\nu$(C≡C) 2079 $cm^{-1}$.

*2.2.8. Synthesis of model compounds **M1**, **M2** and **M3***

A typical procedure was given for the synthesis of **M1** starting from **L1** as follows**:** To a solution of ligand **L1** (5.73 mg, 0.01 mmol) and *trans*-Pt($PEt_3$)$_2$(Ph)Cl (12.00 mg, 0.022 mmol) in triethylamine (3 mL) and $CH_2Cl_2$ (3 mL) was added CuI (1.5 mg) under nitrogen. After stirring overnight at room temperature, all volatile components were removed under reduced pressure. The residue was dissolved in $CH_2Cl_2$ and purified by preparative silica TLC plates using $CH_2Cl_2$/hexane (1:1.5) as eluent to give the pure product **M1** (9 mg, 57%) as a purple solid. $^1$H NMR (400 MHz, $CDCl_3$, δ/ppm): 8.94 (d, $J$ = 4.1 Hz, 2H, Ar), 7.40−7.29 (m, 4H, Ar), 6.99 (t, $J$ = 7.4 Hz, 4H, Ar), 6.95 (d, $J$ = 4.1 Hz, 2H, Ar), 6.82 (t, $J$ = 7.2 Hz, 2H, Ar), 4.04 (t, $J$ = 7.8 Hz, 4H, $C_8H_{17}$), 1.77−1.71 (m, 28H, $PEt_3$+$C_8H_{17}$), 1.42−1.26 (m, 20H, $C_8H_{17}$), 1.14−1.04 (m, 36H, $PEt_3$), 0.87 (t, $J$ = 7.1 Hz, 6H, $C_8H_{17}$); $^{31}$P NMR (162 MHz, $CDCl_3$, δ/ppm): 10.10 ($^1J_{P–Pt}$ = 2617 Hz); FAB-MS: *m/z* 1588.2 $[M+H]^+$; IR (KBr): $\nu$(C≡C) 2074 $cm^{-1}$.

**M2**: Purple solid, yield: 49%. $^1$H NMR (400 MHz, $CDCl_3$, δ/ppm): 8.96 (d, $J$ = 4.1 Hz, 2H, Ar), 7.41−7.29 (m, 4H, Ar), 6.98 (t, $J$ = 7.4 Hz, 4H, Ar), 6.94 (d, $J$ = 4.1 Hz, 2H, Ar), 6.82 (t, $J$ = 7.3 Hz, 2H, Ar), 4.06−3.95 (m, 4H, EH), 1.95−1.90 (m, 2H, EH), 1.78−1.71 (m, 24H, $PEt_3$), 1.43−1.31 (m, 16H, EH), 1.14−1.02 (m, 36H, $PEt_3$), 0.92−0.85 (m, 12H, EH); $^{31}$P NMR (162 MHz, $CDCl_3$, δ/ppm): 10.09 ($^1J_{P–Pt}$ = 2617 Hz); FAB-MS: *m/z* 1588.6 $[M+H]^+$; IR (KBr): $\nu$(C≡C) 2074 $cm^{-1}$.

**M3**: Blue-purple solid, yield, 46%. $^1$H NMR (400 MHz, $CDCl_3$, δ/ppm): 8.92 (d, $J$ =

4.2 Hz, 2H, Ar), 7.41−7.28 (m, 4H, Ar), 7.19 (d, $J$ = 4.2 Hz, 2H, Ar), 7.04 (s, 2H, Ar), 6.98 (t, $J$ = 7.4 Hz, 4H, Ar), 6.81 (t, $J$ = 7.3 Hz, 2H, Ar), 4.11−3.99 (m, 4H, EH), 2.65 (t, $J$ = 7.7 Hz, 4H, $C_6H_{13}$), 1.95−1.92 (m, 2H, EH), 1.79−1.72 (m, 24H, $PEt_3$), 1.66−1.61 (m, 4H, $C_6H_{13}$), 1.39−1.29 (m, 28H, EH +$C_6H_{13}$), 1.14−1.06 (m, 36H, $PEt_3$), 0.93−0.87 (m, 18H, EH+$C_6H_{13}$); $^{31}$P NMR (162 MHz, $CDCl_3$, δ/ppm): 10.27 ($^1J_{P-Pt}$ = 2632 Hz); FAB-MS: *m/z* 1921.2 $[M+H]^+$; IR (KBr): $\nu$(C≡C) 2074 $cm^{-1}$.

*2.3. Device fabrication and characterization*

Silicon wafers (n-type) with a thermal oxide layer (300 nm) were used as substrates. Films of 5 nm chromium (as an adhesion layer) and 40 nm gold were evaporated on the surface of $SiO_2$ through a shadow mask as source and drain electrodes. The channel width (W) and length (L) were 2.0 mm and 0.1 mm, respectively. Organic semiconductors were dissolved in toluene with a concentration of 10 mg $mL^{-1}$. The solutions were stirred for 12 h at 60 °C and then spin-coated onto the substrates, followed by thermal annealing (60 °C) process in a glove box filled with high-purity nitrogen. The solar cell device structure was ITO/PEDOT:PSS/active layer/Al, where the active layer is a blend film of the platinum(II) poly(aryleneethynylene)s **P1−P3** as the electron donor and PCBM or $PC_{71}BM$ as the electron acceptor in a weight ratio of 1:4 or 1:5 (w/w). The ITO glass substrates (10 Ω per square) were cleaned by sonication in toluene, acetone, ethanol and deionized water, dried in an oven, and then cleaned with UV ozone for 300 s. As-received PEDOT:PSS solution was passed through the 0.45 μm filter and spin-coated on patterned ITO substrates at 5000 r.p.m.

for 3 min, followed by baking in $N_2$ at 150 ºC for 15 min. The polymer:PCBM (1:4 by weight) active layer was prepared by spin-coating the chlorobenzene solution (30 mg per mL) at 800 r.p.m. for 2 min. The substrates were dried at room temperature in low vacuum (vacuum oven) for 1 h, and then stored in high vacuum ($10^5$–$10^6$ Torr) overnight. Al electrode (100 nm) was evaporated through a shadow mask to define the active area of the devices (2 mm diameter circle). All the fabrication procedures (except drying, PEDOT:PSS annealing and Al deposition) and cell characterization were performed in air. Power conversion efficiency was determined from *J*–*V* curve measurement (using a Keithley 2400 source meter) under white light illumination (at 100 mW $cm^{-2}$). For white light efficiency measurements, Oriel 66002 solar light simulator with AM1.5 filter was used. The light intensity was measured by a Molectron Power Max 500D laser power meter.

## 3. Results and discussion

### *3.1. Synthesis and characterization*

The general synthetic routes of polymers **P1**−**P3** and model compounds **M1**−**M3** are illustrated in Scheme 1. **DPPT** was prepared by the ring closure reaction between 2-thiophenecarbonitrile and 0.5 equiv of diisopropyl succinate ester in *tert*-amyl alcohol under basic conditions according to the procedure in the literature [40]. Followed by alkylation with 1-bromooctane or 1-bromo-2-ethylhexane, compounds **L1-T** and **L2-T** were obtained in moderate yields, similar to the value reported in the literature [41]. The low yield may be ascribed to the formation of soluble by-products,

which has not been identified since not very pure samples were isolated by column chromatography. Possible side products may be DPP derivatives where O-alkylation of the amide [42] occurred instead of *N*-alkylation or product of ring opening reaction of lactam ring as deduced from FAB-MS (three alkyl groups on one by-product) and asymmetric $^{1}H$ NMR spectra. According to the common method reported in the literature, using NBS as the brominating reagent, the bromination of bithiophene containing DPP was carried out in chloroform at room temperature for two days, but the reaction time was longer and the yield was relatively lower. So, we optimized this reaction condition by using bromine as the brominating reagent and refluxing in chloroform for one hour to achieve compounds **L1-Br** and **L2-Br** in high yields. By Sonogashira coupling reaction, the bromide groups were converted into the corresponding trimethylsilylethynyl groups in a $CH_2Cl_2/NEt_3$ mixture using CuI, $Pd(OAc)_2$ and $PPh_3$ as the catalysts. By following desilylation with potassium carbonate in methanol, the diethynyl ligands **L1** and **L2** were obtained as purple solids. Starting from **L2-Br**, **L3-HT** was prepared by Stille coupling reaction with tributyl(4-hexylthiophen-2-yl)stannane in dry toluene, using $Pd(PPh_3)_4$ as a catalyst. **L3-HT** can be easily brominated by NBS, and followed by Sonogashira coupling reaction and desilylation reaction to afford the diethynyl ligand **L3** as a deep purple solid. Polymers **P1−P3** and their model compounds **M1−M3** were prepared by the Sonogashira-type dehydrohalogenation between each of the diethynyl precursors and the corresponding platinum precursors *trans*-$Pt(PBu_3)_2Cl_2$ and *trans*-$Pt(PEt_3)_2(Ph)Cl$ with the stoichiometric ratio of 1:1 and 1:2.1, respectively. Polymers **P1−P3** were

purified by flash column chromatography over neutral $Al_2O_3$ to remove ionic impurities and catalyst residues, and repeated precipitation and isolation.

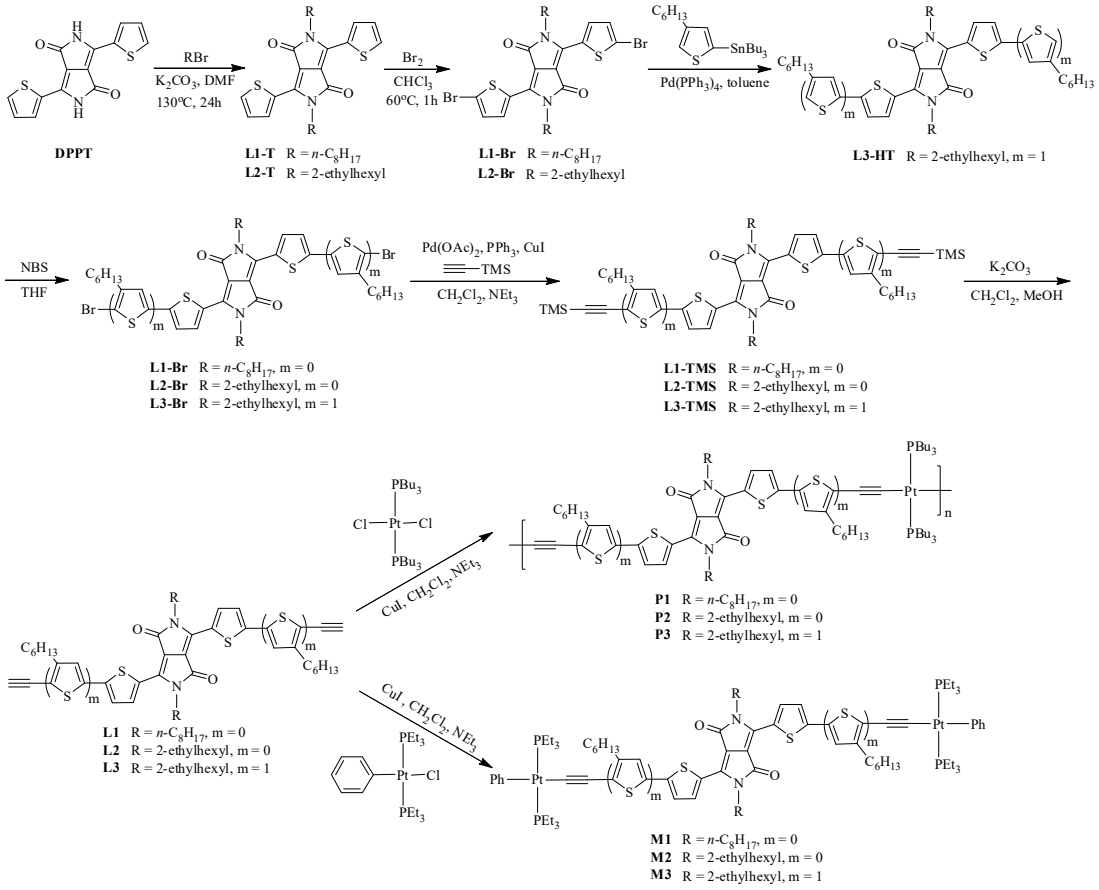


**Scheme 1.** Synthetic pathways of model compounds **M1**−**M3** and polymers **P1**−**P3**.

Model compounds **M1**−**M3** and platinum(II) polymers **P1**−**P3** were fully characterized by common spectroscopic techniques including infrared (IR) and NMR ($^1$H, $^{13}$C and $^{31}$P) spectroscopies, and FAB mass spectrometry. The strong single $^{31}$P signal flanked with two satellites for platinum(II) polymers and model compounds is consistent with a *trans*-geometry of the $Pt(PBu_3)_2$ and $Pt(PEt_3)_2Ph$ units in a square-planar geometry. More importantly, the $^1J_{P\text{-}Pt}$ values of 2302−2332 Hz for the $PBu_3$ moieties and 2617−2632 Hz for the $PEt_3$ moieties are typical of those for related

*trans*-$PtP_2$ systems, which are smaller than those of the *cis*-isomers (> 3500 Hz) [43]. The FT-IR spectra show that $\nu$(C≡C) stretching frequencies of platinum-containing polymers **P1−P3** are located at ~ 2079 $cm^{-1}$ and **M1−M3** at ~2074 $cm^{-1}$, which are lower than those for the terminal acetylenic C≡C−H stretching vibrations at 2091−2098 $cm^{-1}$. It may be attributed to either the metal-to-alkyne π back bonding or the $M^{\delta+}-C^{\delta-}$ polarity leading to a higher degree of conjugation formed in the former [44].

Molecular weights and polydispersity indices (PDIs) of the polymers were determined by gel permeation chromatography (GPC) analysis with a polystyrene standard calibration. The GPC results are summarized in Table 1. **P2** exhibits a high weight-average molecular weight ($M_w$) of 164.3 kg/mol with a PDI of 2.67. The other two polymers have relatively lower $M_w$ of 118.8 kg/mol with a PDI of 2.45 for **P1** and 48.9 kg/mol with a PDI of 2.21 for **P3**. The difference of the molecular weights may be resulted from the reactivity and steric hindrance of the donor segments as well as solubility of ligands. The PDI values may be optimized by repeating the precipitation of polymers. Molecular weight of polymer is also a key factor affecting the performance of polymer solar cells [45].

**Table 1.** GPC and TGA results for platinum polyyne polymers **P1−P3**.

| Polymer | $M_n$ | $M_w$ | PDI | DP | $T_{dec}$ (°C) |
|---|---|---|---|---|---|
| **P1** | 48490 | 118800 | 2.45 | 41 | 320 |
| **P2** | 61560 | 164320 | 2.67 | 53 | 344 |
| **P3** | 22160 | 48940 | 2.21 | 15 | 283 |

*3.2. Thermal properties*

Thermal gravimetric analysis (TGA) data under nitrogen show that polymers **P1**−**P3** exhibit good thermal stability with onset decomposition temperatures ($T_{dec}$) at 320, 344 and 283 °C, respectively, and the percent weight loss of 17.8−30.3% indicate the removal of one $PBu_3$ and one to three Bu groups from their polymers in the decomposition step. This level of thermal stability is adequate to meet the requirement of optoelectronic device engineering.

*3.3. Optical properties*

The normalized UV-vis absorption and photoluminescence (PL) spectra of Pt(II) polyyne polymers **P1**−**P3** in $CH_2Cl_2$ solution are shown in Figs. 2 and 3. The detailed optical data are summarized in Table 2. Polymers **P1**−**P3** show two sets of weak absorption peaks in the range of 310−500 nm corresponding to the π-π* transition and strong absorption peaks between 500 and 750 nm due to the ICT effect between the donor units (thiophene) and the central acceptor unit (DPP). **P1** and **P2** show similar absorption spectra with the absorption maxima at 652 and 654 nm, respectively, presumably due to the very similar structure except for the substituted alkyl groups at the N-atom of lactam. The absorption maximum of **P3** shows a significant red shift of 28−30 nm and the absorption band was simultaneously broadened compared with those of **P1** and **P2**, mostly because the increase of the number of thiophene unit in **P3** results in more extensive π–electron delocalization within the polymer backbone and further enhanced the ICT effect. The similar phenomenon occurs in their corresponding model compounds **M1**−**M3**. The optical bandgaps of these polymers

are 1.69−1.81 eV, as estimated from the absorption onset in the solution state ($E_g^{opt}$ = $1240/\lambda_{abs}^{onset}$ eV).

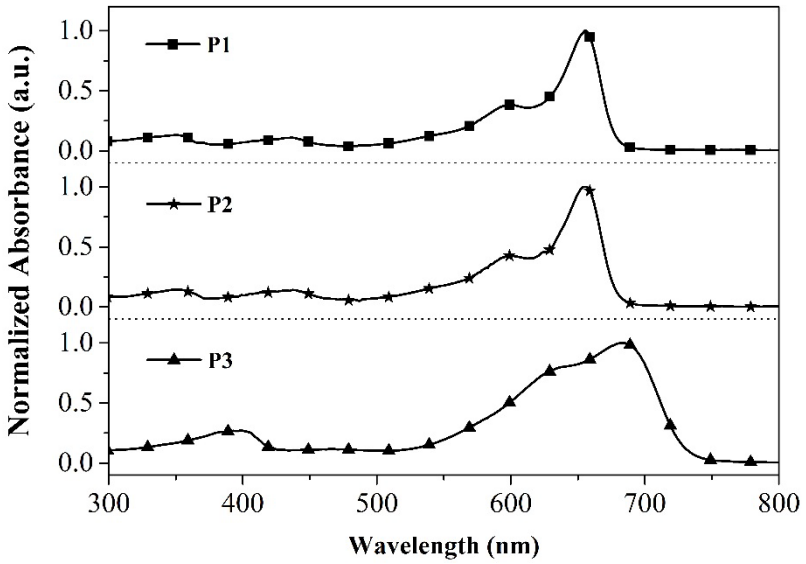


**Fig. 2.** Normalized UV-vis absorption spectra of polymers **P1**−**P3** in $CH_2Cl_2$ at 293 K.

The emission spectra of model compounds **M1**−**M3** and polymers **P1**−**P3** each exhibit a strong peak with a concomitant shoulder peak at the longer wavelength. With the extension of π-conjugated system from model compounds to the corresponding polymers, obvious red shifts are observed in their emission spectra. The photoluminescence (PL) maxima of **P1**, **P2** and **P3** occur at 678, 676 and 731 nm, respectively, originated from their ICT excited state. The PL quantum yields of **P1**−**P3** in $CH_2Cl_2$ relative to Rhodamine 6G in ethanol were calculated to be only 1−2%. The emission density of **P1**−**P3** significantly decreased compared with those of the ligands and model compounds, as deduced from the reduced quantum yield values, mostly because an ICT excited state contributes to the efficient photoinduced charge separation in energy conversion for **P1**−**P3** [23,46]. Moreover, the small Stokes shift

and short lifetime of DPP-based polymers illustrate that the emission process should be assigned to the fluorescence.

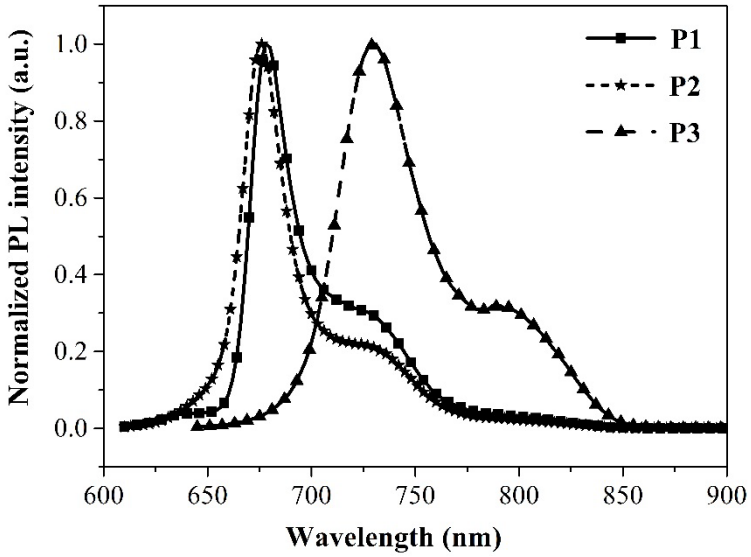


**Fig. 3.** Normalized PL spectra of polymers **P1**−**P3** in $CH_2Cl_2$ at 293 K.

**Table 2.** Photophysical data for diethynyl ligands **L1**−**L3**, model complexes **M1**−**M3** and polymers **P1**−**P3** in $CH_2Cl_2$ at 293 K.

| | $\lambda_{abs}$ [nm] ($\varepsilon \times 10^4$ $M^{-1}$ $cm^{-1}$) | $\lambda_{emi}$ [nm] ($\tau_F$, ns) | $\Phi_F$ (%)[a] |
|---|---|---|---|
| **L1** | 316 (3.4), 545 (3.2), 588 (3.9) | 604 (5.94), 653 (6.15) | 27 |
| **L2** | 318 (3.0), 546 (2.9), 587 (3.2) | 605 (6.34), 654 (5.35) | 34 |
| **L3** | 368 (3.2), 594 (6.0), 631 (6.1) | 665 (2.13), 723 (2.23) | 6 |
| **M1** | 344 (0.8), 438 (0.5), 584 (2.6), 635 (4.0) | 654 (3.53), 706 (3.65) | 18 |
| **M2** | 344 (1.5), 438 (1.0), 585 (4.3), 636 (6.4) | 653 (3.66), 707 (4.31) | 24 |
| **M3** | 399 (1.3), 638 (4.8),676 (5.5) | 724 (1.15), 790 (0.44) | 2 |
| **P1** | 434, 598, 652 | 678 (0.60), 723 (0.75) | 1 |
| **P2** | 436, 598, 654 | 676 (0.89), 725 (1.00) | 2 |
| **P3** | 399, 638, 682 | 731 (0.85), 791 (1.11) | 1 |

[a] Quantum yields were measured with an excitation wavelength of 488 nm using rhodamine 6G in ethanol as reference ($\Phi_F$ = 0.95).

*3.4. Electrochemical properties*

Cyclic voltammetry was widely employed to estimate the highest occupied molecular orbital (HOMO) and the lowest unoccupied molecular orbital (LUMO) levels of conjugated polymers. The relevant data are outlined in Table 3. All materials exhibit irreversible oxidation and reduction process. From the onset values of oxidation and reduction potentials in the cyclic voltammograms, the HOMO and LUMO levels of the polymers were calculated according to the following equations $E_{HOMO} = -(E_{ox} + 4.72)$ eV and $E_{LUMO} = -(E_{red} + 4.72)$ eV [47,48], respectively. **P1** and **P2** have very similar HOMO and LUMO energy levels, probably because the substituted alkyl groups can only control the solubility and have no effect on the energy levels of the polymers. In comparison with **P2**, the HOMO energy level of **P3** is slightly higher and the LUMO energy level is decreased as a result of the introduction of additional 3-hexylthiophene unit, which results in the lower electrochemical bandgap. The electrochemical bandgaps of **P1**−**P3** seem somewhat larger than the corresponding optical bandgaps within the range of error (0.21−0.27 eV).

**Table 3.** Electrochemical data and frontier orbital energy levels for **P1**−**P3**.[a]

| Polymer | $E_{ox}^{onset}/E_{HOMO}$ | $E_{red}^{onset}/E_{LUMO}$ | $E_g^{ec}$ | $E_g^{opt}$ |
|---|---|---|---|---|
| | (V)/(eV) | (V)/(eV) | (eV) | (eV) |
| **P1** | 0.79 / −5.51 | −1.23 / −3.49 | 2.02 | 1.81 |
| **P2** | 0.79 / −5.51 | −1.24 / −3.48 | 2.03 | 1.81 |
| **P3** | 0.77 / −5.49 | −1.18 / −3.54 | 1.96 | 1.69 |

[a] $E_{ox}$: onset oxidation potential vs. Ag/AgCl, and $E_{HOMO} = -(E_{ox} + 4.72)$ eV; $E_{red}$: onset reduction potential vs. Ag/AgCl, and $E_{LUMO} = -(E_{red} + 4.72)$ eV; $E_g^{ec} = E_{LUMO} - E_{HOMO} = E_{ox} - E_{red}$.

*3.5. Hole mobility from field-effect transistor characteristics*

The charge carrier mobilities of solution-processed DPP-based organometallic polymers thin films were measured in field-effect transistors (FET) devices using the most basic bottom-gate top-contact architecture with evaporated gold source and drain electrodes and $SiO_2$/Si++ substrates. The three polymers **P1**−**P3** exhibit a clear signature of p-channel semiconductor behavior, and their hole mobilities were 1.15 × $10^{-5}$, 1.28 × $10^{-5}$, 9.61× $10^{-6}$ $cm^2$ $V^{-1}$ $s^{-1}$, respectively. Polymer **P2** with branched 2-ethylhexyl side chain shows a slightly higher hole mobility than that of **P1** with linear *n*-octyl group, which is probably due to the higher molecular weight and better solubility in organic solvents for **P2**, rendering its better quality thin films.

*3.6. Performance of BHJ solar cells*

Fig. 4 shows the *J*−*V* curves of the devices based on DPP-based platinum(II) polyyne polymers and [6,6]phenyl-$C_{61}$-butyric acid methyl ester (PCBM). The photovoltaic parameters including open circuit voltage ($V_{oc}$), short circuit density ($J_{sc}$), fill factor (FF) and PCE are summarized in Table 4. The BHJ device based on **P1** blended with PCBM (1:4) achieved a PCE of 1.4% with $V_{oc}$ of 0.75 V, $J_{sc}$ of 5.45 mA $cm^{-2}$ and FF of 0.34. **P2** and **P3** devices exhibited significantly lower $J_{sc}$ and relatively lower $V_{oc}$, leading to the lower PCE. This result may be attributed to the substituted alkyl groups at the N-atom of lactam. The linear alkyl chain allows the well-organized arrangement between the polymer backbones by reducing the π-π stacking distances and thus facilitates the charge transfer and obtains a higher $J_{sc}$ for **P1** compared with

**P2** and **P3** with branched alkyl groups. The better absorption properties of **P3** over **P2** with longer thiophene length also resulted in a slightly enhanced device efficiency.

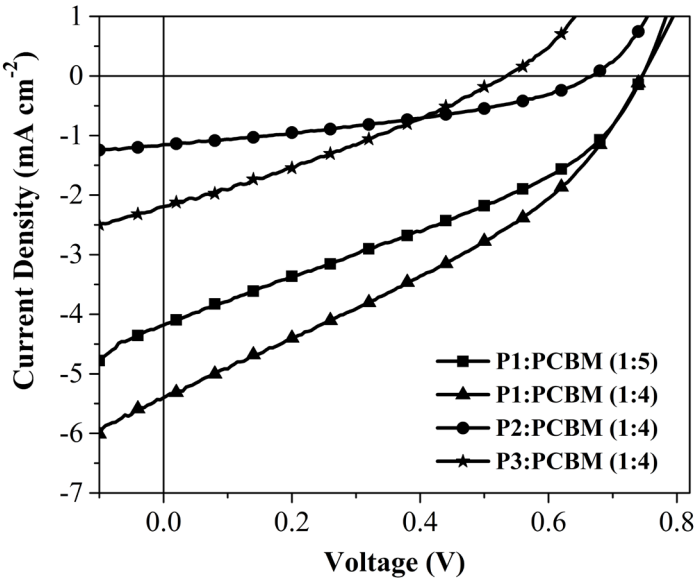


**Fig. 4.** *J*−*V* curves of devices with **P1**−**P3**:PCBM (1:4 or 1:5) active layers under AM 1.5G illumination.

The $V_{oc}$ of DPP-based organometallic polymers **P1**−**P3** was found to be 0.75, 0.67 and 0.54 eV, respectively. The observed trend is not consistent with the very similar HOMO energy levels of **P1**−**P3**, probably because the energetically expected $V_{oc}$ value can be modified by other parameters such as carrier recombination, bulkiness of side chains and morphology of the photoactive layer [49−51]. The real origin of $V_{oc}$ in BHJ device is still under intense debate.

**Table 4.** Photovoltaic performance of the BHJ devices based on **P1**−**P3**.

| Device[a] | $V_{oc}$ (V) | $J_{sc}$ (mA cm$^{-2}$) | FF | PCE (%) |
|---|---|---|---|---|
| **P1**:PCBM (1:4) | 0.75 | 5.45 | 0.34 | 1.40 |
| **P1**:PCBM (1:5) | 0.75 | 4.26 | 0.35 | 1.11 |
| **P2**:PCBM (1:4) | 0.67 | 1.13 | 0.37 | 0.28 |

| | | | | |
|---|---|---|---|---|
| **P3**:PCBM (1:4) | 0.54 | 2.23 | 0.30 | 0.36 |

[a] The numbers in parentheses denote the ratio of polymer:PCBM (w/w).

## 4. Conclusion

A new series of conjugated DPP-based platinum polyyne polymers has been synthesized by the Sonogashira-type coupling polymerization and systematically characterized. By introducing branched side chains, the solubility of organometallic polymer could be remarkably improved. In addition, the extension of conjugation length by increasing the additional 3-hexylthiophene ring also enhanced the visible absorption properties of polymer, because a stronger ICT effect could be formed between the extended donor and DPP units. The PCE of 1.4% was achieved in the BHJ device based on **P1**:PCBM (1:4) with $V_{oc}$ of 0.75 V, $J_{sc}$ of 5.45 mA cm$^{-2}$ and FF of 0.34. Without the loss of solubility, linear alkyl side chains on polymers could be used to promote the nanostructural order of the active layer and further improve the photovoltaic performance.

Apart from the properties discussed above, the morphology of the active layer is a critical factor in controlling the performance of BHJ solar cells even if the donor (polymer) and acceptor (fullerene or non-fullerene) have ideal electronic relationship and absorption properties. Therefore, the performance of these devices could be further improved by device optimization including solvent choice, solvent additives, non-fullerene acceptors as well as inverted device structures.

**Acknowledgements**

W.-Y.W. thanks the Hong Kong Research Grants Council (PolyU 123384/16P) and the Hong Kong Polytechnic University (1-ZE1C and 847S) for the financial support. Q.L. thanks the National Natural Science Foundation of China (51803002) and the Natural Science Foundation of Anhui Province (1708085QE93) and overseas students' innovative project funding scheme of Anhui Province.

**References**

[1] A. Polman, M. Knight, E.C. Garnett, B. Ehrler, W.C. Sinke, Photovoltaic materials: Present efficiencies and future challenges, Science 352 (2016) aad4424.

[2] J. Hou, O. Inganäs, R.H. Friend, F. Gao, Organic solar cells based on non-fullerene acceptors, Nat. Mater. 17 (2018) 119–128.

[3] Z. Xiao, X. Jia, L. Ding, Ternary organic solar cells offer 14% power conversion efficiency, Sci. Bull. 62 (2017) 1562–1564.

[4] J.B. Zhao, Y.K. Li, G.F. Yang, K. Jiang, H.R. Lin, H. Ade, W. Ma, H. Yan, Efficient organic solar cells processed from hydrocarbon solvents, Nat. Energy 1 (2016) 15027.

[5] H.T. Fu, Z.H. Wang, Y.M. Sun, Polymer donors for high-performance non-fullerene organic solar cells, Angew. Chem. Int. Ed. 58 (2019) 4442–4453.

[6] L.Y. Lu, T.Y. Zheng, Q.H. Wu, A.M. Schneider, D.L. Zhao, L.P. Yu, Recent advances in bulk heterojunction polymer solar cells, Chem. Rev. 115 (2015) 12666–12731.

[7] H.X. Zhou, L.Q. Yang, W. You, Rational design of high performance conjugated polymers for organic solar cells, Macromolecules 45 (2012) 607–632.

[8] L.T. Dou, Y.S. Liu, Z.R. Hong, G.Li, Y. Yang, Low-bandgap near-IR conjugated polymers/molecules for organic electronics, Chem. Rev. 115 (2015) 12633–12665.

[9] C.B. Nielsen, S. Holliday, H.-Y. Chen, S.J. Cryer, I. McCulloch, Non-fullerene electron acceptors for use in organic solar cells, Acc. Chem. Res. 48 (2015) 2803–2812.

[10] H.F. Yao, L. Ye, H. Zhang, S.S. Li, S.Q. Zhang, J.H. Hou, Molecular design of benzodithiophene-based organic photovoltaic materials, Chem. Rev. 116 (2016) 7397–7457.

[11] G. Li, V. Shrotriya, J.S. Huang, Y. Yao, T. Moriarty, K. Emery, Y. Yang, High-efficiency solution processable polymer photovoltaic cells by self-organization of polymer blends, Nat. Mater. 4 (2005) 864–868.

[12] S.Q. Zhang, L.Ye, J.H. Hou, Breaking the 10% efficiency barrier in organic photovoltaics: morphology and device optimization of well-known PBDTTT polymers, Adv. Energy Mater. 6 (2016) 1502529.

[13] L.Ye, X.C. Jiao, S.Q. Zhang, H.F. Yao, Y.P. Qin, H. Ade, J.H. Hou, Control of mesoscale morphology and photovoltaic performance in diketopyrrolopyrrole-based small bandgap terpolymers, Adv. Energy Mater. 7 (2017) 1601138.

[14] J. Peet, J.Y. Kim, N.E. Coates, W.L. Ma, D. Moses, A.J. Heeger, G.C. Bazan, Efficiency enhancement in low-bandgap polymer solar cells by processing with alkane dithiols, Nat. Mater. 6 (2007) 497–500.

[15] L.X. Meng, Y.M. Zhang, X.J. Wan, C.X. Li, X. Zhang, Y.B. Wang, X. Ke, Z. Xiao, L.M. Ding, R.X. Xia, H.-L. Yip, Y. Cao, Y.S. Chen, Organic and solution-processed tandem solar cells with 17.3% efficiency, Science 361 (2018) 1094–1098.

[16] G. Li, W.-H. Chang, Y. Yang, Low-bandgap conjugated polymers enabling solution-processable tandem solar cells, Nat. Rev. Mater. 2 (2017) 17043.

[17] X.Z. Che, Y.X. Li, Y. Qu, S.R. Forrest, High fabrication yield organic tandem

photovoltaics combining vacuum- and solution-processed subcells with 15% efficiency, Nat. Energy 3 (2018) 422–427.

[18] C.E. Small, S. Chen, J. Subbiah, C.M. Amb, S.W. Tsang, T.H. Lai, J. Reynolds, R.F. So, High-efficiency inverted dithienogermole-thienopyrrolodione-based polymer solar cells, Nat. Photon. 6 (2012) 115–120.

[19] Z. He, C. Zhong, S. Su, M. Xu, H. Wu, Y. Cao, Enhanced power-conversion efficiency in polymer solar cells using an inverted device structure, Nat. Photon. 6 (2012) 591–595.

[20] S.S. Li, L. Ye, W.C. Zhao, H.P. Yan, B. Yang, D.L. Liu, W.N. Li, H. Ade, J.H. Hou, A wide band gap polymer with a deep highest occupied molecular orbital level enables 14.2% efficiency in polymer solar cells, J. Am. Chem. Soc. 140 (2018) 7159–7167.

[21] S.Q. Zhang, Y.P. Qin, J. Zhu, J.H. Hou, Over 14% efficiency in polymer solar cells enabled by a chlorinated polymer donor, Adv. Mater. 30 (2018) 1800868.

[22] B. Kan, H.R. Feng, H.F. Yao, M.J. Chang, X.J. Wan, C.X. Li, J.H. Hou, Y.S. Chen, A chlorinated low-bandgap small-molecule acceptor for organic solar cells with 14.1% efficiency and low energy loss, Sci. China Chem. 61 (2018) 1307–1313.

[23] W.Y. Wong, X.Z. Wang, Z. He, A.B. Djurišić, C.T. Yip, K.Y. Cheung, H. Wang, C.S.K. Mak, W.K. Chan, Metallated conjugated polymers as a new avenue towards high-efficiency polymer solar cells, Nat. Mater. 6 (2007) 521–527.

[24] W.Y. Wong, X.Z. Wang, Z. He, K.K. Chan, A.B. Djurišić, K.Y. Cheung, C.T. Yip, A.M.C. Ng, Y.Y. Xi, C.S.K. Mak, W.K. Chan, Tuning the absorption, charge transport

properties, and solar cell efficiency with the number of thienyl rings in platinum-containing poly(aryleneethynylene)s, J. Am. Chem. Soc. 129 (2007) 14372–14380.

[25] N.S. Baek, S.K. Hau, H.L. Yip, O. Acton, K.S. Chen, A.K.Y. Jen, High performance amorphous metallated π-conjugated polymers for field-effect transistors and polymer solar cells, Chem. Mater. 20 (2008) 5734–5736.

[26] L. Ye, S.Q. Zhang, W. Ma, B.H. Fan, X. Guo, Y. Huang, H. Ade, J.H. Hou, From binary to ternary solvent: morphology fine-tuning of D/A blends in PDPP3T-based polymer solar cells, Adv. Mater. 4 (2012) 6335–6341.

[27] A.T. Yiu, P.M. Beaujuge, O.P. Lee, C.H. Woo, M.F. Toney, J.M.J. Fréchet, Side-chain tunability of furan-containing low-band-gap polymers provides control of structural order in efficient solar cells, J. Am. Chem. Soc. 34 (2012) 2180–2185.

[28] K.H. Hendriks, G.H.L. Heintges, V.S. Gevaerts, M.M. Wienk, R.A.J. Janssen, High-molecular-weight regular alternating diketopyrrolopyrrole-based terpolymers for efficient organic solar sells, Angew. Chem. Int. Ed. 52 (2013) 8341–8344.

[29] G.G. Qiu, Z.Y. Jiang, Z.J. Ni, H.L. Wang, H.L. Dong, J.Q. Zhang, X.T. Zhang, Z.B. Shu, K. Lu, Y. Zhen, Z.X. Wei, W.P. Hu, Asymmetric thiophene/pyridine flanked diketopyrrolopyrrole polymers for high performance polymer ambipolar field-effect transistors and solar cells, J. Mater. Chem. C 5 (2017) 566–572.

[30] L. Burgi, M. Trubiez, R. Pfeiffer, F. Bienewald, H.J. Kirner, C. Winnewisser, High-mobility ambipolar near-infrared light-emitting polymer field-effect transistors, Adv. Mater. 20 (2008) 2217–2224.

[31] W.W. Li, K.H. Hendriks, M.M. Wienk, R.A.J. Janssen, Diketopyrrolopyrrole polymers for organic solar cells, Acc. Chem. Res. 49 (2016) 78–85.

[32] X.X. Chen, Z.J. Zhang, Z.C. Ding, J. Liu, L.X. Wang, Diketopyrrolopyrrole-based conjugated polymers bearing branched oligo(ethylene glycol) side chains for photovoltaic devices, Angew. Chem. Int. Ed. 55 (2016) 10376–10380.

[33] I. Meager, R.S. Ashraf, S. Mollinger, B.C. Schroeder, H. Bronstein, D. Beatrup, M.S. Vezie, T. Kirchartz, A. Salleo, J. Nelson, I. McCulloch, Photocurrent enhancement from diketopyrrolopyrrole polymer solar cells through alkyl-chain branching point manipulation, J. Am. Chem. Soc. 135 (2013) 11537–11540.

[34] L.T. Dou, J. Gao, E. Richard, J.B. You, C.C. Chen, K.C. Cha, Y.J. He, G. Li, Y. Yang, Systematic investigation of benzodithiophene- and diketopyrrolopyrrole-based low-bandgap polymers designed for single junction and tandem polymer solar cells, J. Am. Chem. Soc. 134 (2012) 10071–10079.

[35] R.S. Ashraf, I. Meager, M. Nikolka, M. Kirkus, M. Planells, B.C. Schroeder, S. Holliday, M. Hurhangee, C.B. Nielsen, H. Sirringhaus, I. McCulloch, Chalcogenophene comonomer comparison in small band gap diketopyrrolopyrrole-based conjugated polymers for high-performing field-effect transistors and organic solar cells, J. Am. Chem. Soc. 137 (2015) 1314–1321.

[36] B. Sun, W. Hong, Z. Yan, H. Aziz, Y. Li, Record high electron mobility of 6.3 $cm^2 V^{-1} s^{-1}$ achieved for polymer semiconductors using a new building block, Adv. Mater. 26 (2014) 2636–2642.

[37] B. Walker, A.B. Tamayo, X.D. Dang, P. Zalar, J.H. Seo, A. Garcia, M. Tantiwiwat, T.Q. Nguyen, Nanoscale phase separation and high photovoltaic efficiency in solution-processed, small-molecule bulk heterojunction solar cells, Adv. Funct. Mater. 9 (2009) 3063–3069.

[38] A.L. Tang, C.L. Zhan, J.N. Yao, E.J. Zhou, Design of diketopyrrolopyrrole (DPP)-based small molecules for organic-solar-cell applications, Adv. Mater. 29 (2017) 1600013.

[39] J. Chatt, B.L. Shaw, Alkyls and aryls of transition metals, Part II. Platinum(II) derivatives, J. Chem. Soc. (1959) 4020–4033.

[40] Y.N. Li, Diketopyrrolopyrrole-based derivatives for thin film transistors, EP2034537 A2, 2009.

[41] S. Stas, S. Sergeyev, Y. Geerts, Synthesis of diketopyrrolopyrrole (DPP) derivatives comprising bithiophene moieties, Tetrahedron 66 (2010) 1837–1845.

[42] B.C. Challis, J.A. Challis, Reactions of the carboxamide group, in: J. Zabicky (Eds.), The Chemistry of Amides, Wiley, New York, 1970, pp.734–848.

[43] S.O. Grim, R.L. Keiter, W. McFarlane, A phosphorus-31 nuclear magnetic resonance study of tertiary phosphine complexes of platinum(II), Inorg. Chem. 6 (1967) 1133–1137.

[44] J. Lewis, N.J. Long, P.R. Raithby, G.P. Schields, W.Y. Wong, M.J. Younus, Synthesis and characterisation of new acetylide-functionalised oligothiophenes and their dinuclear platinum complexes, J. Chem. Soc. Dalton Trans. (1997) 4283–4288.

[45] M.C. Scharber, D. Muhlbacher, M. Koppe, P. Denk, C. Waldauf, A.J. Heeger, C.J.

Brabec, Design rules for donors in bulk-heterojunction solar cells−Towards 10% energy-conversion efficiency, Adv. Mater. 18 (2006) 789–794.

[46] B. Miehlich, A. Savin, H. Stoll, H. Preuss, Results obtained with the correlation energy density functionals of Becke and Lee, Yang and Parr, Chem. Phys. Lett. 157 (1989) 200–206.

[47] J.H. Hou, Z.A. Tan, Y. Yan, Y.J. He, C.H. Yang, Y.F. Li, Synthesis and photovoltaic properties of two-dimensional conjugated polythiophenes with bi(thienylenevinylene) side chains, J. Am. Chem. Soc. 128 (2006) 4911–4916.

[48] C.G. Van de Walle, J. Neugebauer, Universal alignment of hydrogen levels in semiconductors, insulators and solutions, Nature 423 (2003) 626–628.

[49] M.D. Perez, C. Borek, S.R. Forrest, M.E. Thompson, Molecular and morphological influences on the open circuit voltages of organic photovoltaic devices, J. Am. Chem. Soc. 131 (2009) 9281–9286.

[50] K. Vandewal, K. Tvingstedt, A. Gadisa, O. Inganas, J.V. Manca, On the origin of the open-circuit voltage of polymer-fullerene solar cells, Nat. Mater. 8 (2009) 904–909.

[51] L.Q. Yang, H.X. Zhou, W. You, Quantitatively analyzing the influence of side chains on photovoltaic properties of polymer-fullerene solar cells, J. Phys. Chem. C 114 (2010) 16793–16800.